Strong Dependence of Mechanical Properties on Fiber Diameter for Polymer−Nanotube Composite Fibers: Differentiating Defect from Orientation Effects

Karen Young,[†] Fiona M. Blighe,[†] Juan J. Vilatela,[‡] Alan H. Windle,[‡] Ian A. Kinloch,[§] Libo Deng,[§] Robert J. Young,[§] and Jonathan N. Coleman[†,⊥,*]

[†]School of Physics, Trinity College Dublin, University of Dublin, Dublin 2, Ireland, [‡]Department of Materials Science and Metallurgy, University of Cambridge, Pembroke Street, Cambridge CB2 3QZ, United Kingdom, [§]North West Composite Centre and School of Materials, University of Manchester, Manchester M13 9PL, United Kingdom, and [⊥]Centre for Research on Adaptive Nanostructures & Nanodevices, Trinity College Dublin, University of Dublin, Dublin 2, Ireland

ABSTRACT We have prepared polyvinylalcohol−SWNT fibers with diameters from ~1 to 15 μm by coagulation spinning. When normalized to nanotube volume fraction, V_f, both fiber modulus, Y, and strength, σ_B, scale strongly with fiber diameter, D: $Y/V_f \propto D^{-1.55}$ and $\sigma_B/V_f \propto D^{-1.75}$. We show that much of this dependence is attributable to correlation between V_f and D due to details of the spinning process: $V_f \propto D^{0.93}$. However, by carrying out Weibull failure analysis and measuring the orientation distribution of the nanotubes, we show that the rest of the diameter dependence is due to a combination of defect and orientation effects. For a given nanotube volume fraction, the fiber strength scales as $\sigma_B \propto D^{-0.29}D^{-0.64}$, with the first and second terms representing the defect and orientation contributions, respectively. The orientation term is present and dominates for fibers of diameter between 4 and 50 μm. By preparing fibers with low diameter (1−2 μm), we have obtained mean mechanical properties as high as $Y = 244$ GPa and $\sigma_B = 2.9$ GPa.

KEYWORDS: polymer−nanotube composite · fiber · strength · modulus · defect · orientation

Alongside graphene, carbon nanotubes are among the stiffest and strongest materials known to man. For well-graphitized single-walled nanotubes (SWNTs), the Young's modulus has consistently been reported as close to 1 TPa while the tensile strength is thought to be in the range of 50−150 GPa.[1−7] Because of these superlative mechanical properties and due to their one-dimensional nature, SWNTs are considered to be the ultimate filler for reinforced composite fibers.[8−23] The simplest possible model to describe the mechanical properties of composite fibers is the rule of mixtures, which predicts that the fiber modulus, Y, and strength, σ_B, are given by[7,24−26]

$$Y = (\eta_o\eta_{LY}Y_{NT} - Y_P)V_f + Y_P \approx \eta_o\eta_{LY}Y_{NT}V_f \quad (1)$$

$$\sigma_B = (\eta_o\eta_{L\sigma}\sigma_{NT} - \sigma_P)V_f + \sigma_P \approx \eta_o\eta_{L\sigma}\sigma_{NT}V_f \quad (2)$$

Here the subscripts NT and P refer to nanotube and polymer, respectively. In addition, η_o and η_L are factors which vary between 0 and 1 and correct for the effects of nanotube orientation and length, respectively.[19,24] (Note, η_L takes different forms for modulus and strength; η_{LY} and $\eta_{L\sigma}$. In addition, $\eta_{L\sigma}$ has two forms depending on whether the nanotube length is greater or less than the critical length.)[25] The approximations are accurate for appreciable nanotube volume fractions and when the polymer modulus and strength are significantly lower than those of the nanotubes. The latter condition is not generally true for high-performance polymers such as PBO.[15] However, for coagulation spun fibers such as those studied here, the polymer chains are likely to be weakly aligned, resulting in relatively low values of Y_P and σ_P. We have recently shown this approximation to hold very well for PVA−SWNT coagulation spun fibers with diameters of 5−10 μm.[27] This means that the maximum possible rate of increase of stiffness or strength with nanotube volume fraction is just the nanotube stiffness or strength: $dY/dV_f \approx Y_{NT}$ or $d\sigma_B/dV_f \approx \sigma_{NT}$ (*i.e.*, when $\eta_o = \eta_L = 1$). Thus, it should be possible to prepare polymer−nanotube composites with $dY/dV_f \approx 1$ TPa and $d\sigma_B/dV_f \approx 100$ GPa. If appreciable volume fractions can be achieved, excellent fibers are to be expected.

*Address correspondence to colemaj@tcd.ie.

Received for review August 17, 2010 and accepted October 03, 2010.

Published online October 14, 2010.
10.1021/nn102059c

However, such exceptional properties are not generally obtained. While a number of papers have described fibers with $dY/dV_f > 400$ GPa (see table in ref 28, maximum 1270 GPa[9]), only two papers have described fibers with $d\sigma_B/dV_f > 40$ GPa (56[29] and ~116[30] GPa). In fact, much of the reinforcement observed in the latter paper can be attributed to the effect of nanotube-nucleated crystallinity.[7,26] It is important to point out that very strong composite fibers have been produced; strengths of up to 4.2 GPa have been observed.[15] However, such fibers have only been produced by reinforcing already strong polymers at high loading levels, resulting in relatively low values of $d\sigma_B/dV_f$. Thus, the question remains: Why is it straightforward to prepare composites with dY/dV_f approaching 1 TPa but very difficult to prepare fibers with $d\sigma_B/dV_f$ approaching 100 GPa?

It is generally thought that fiber strength is limited by nanotube length and the strength of the polymer nanotube interface[24,31] (or polymer shear strength in some cases[27,32]). While these are always limiting factors, two other parameters are critically important and perhaps slightly overlooked: the effect of nanotube orientation and the presence of defects. Fibers with greater nanotube alignment have higher η_o and so higher Y and σ_B. A number of papers have shown that drawing improves nanotube alignment and therefore the mechanical properties.[7,27,28] However, detailed studies comparing Y and σ_B to parameters that describe the nanotube orientation distribution have been lacking. A systematic study comparing Y and σ_B to η_o, for example, has yet to be published.[27] More generally, materials failure is very often related to the presence of defects. However, only a very small number of studies have been carried out to investigate the role of defects in polymer−nanotube fiber fracture mechanics.[16] These factors have never been considered together, and their relative importance is not known.

In this work, we prepare composite fibers from polyvinylalcohol (PVA) and SWNTs by coagulation spinning. We measure Y and σ_B for a range of fiber diameters from ~1 to ~15 μm. When normalized to nanotube volume fraction, we observe power law scaling for both modulus and strength with diameter. By performing Weibull analysis on fracture stress data, we show that the presence of surface defects can explain approximately one-third of the diameter dependence of the fiber strength. By measuring the relationship between nanotube orientation and fiber diameter, we show that orientation effects can explain the other two-thirds of the diameter dependence of the fiber strength and all of the diameter dependence of the fiber modulus.

RESULTS

Fiber Formation. Polyvinylalcohol−SWNT fibers were prepared by coagulation spinning.[12,18,22,23,33−38] This involves the injection of a surfactant-stabilized nanotube suspension into the center of a glass pipe through which an aqueous polyvinylalcohol (PVA) solution was flowing.[34] Detailed analysis of the suspension showed it to contain individual nanotubes and small bundles (mean diameter, $\langle d \rangle = 1.8$ nm and mean length $\langle l \rangle = 315$ nm; see Figure S1 in Supporting Information). Exposure of the dispersed SWNTs to the polymer solution results in destabilization of the suspension, resulting in the formation of a fiber. These fibers were collected on a mandrel in a rotating water bath. On removal from the bath, the fibers contained large quantities of water. In some cases, the fibers were drawn in this wet state to a range of draw ratios, DR (DR $= (L - L_0)/L_0$). All fibers were dried initially at ambient conditions and then under vacuum for 48 h. In all cases, the dried fiber diameter, D, was measured at typically 20 positions along the length using a profilometer (Dektak 6 M Stylus Profiler). For all fibers, the nanotube mass fraction was measured by thermogravimetric analysis.[27] This was then converted to volume fraction, V_f, using $\rho_{SWNT} = 1800$ kg/m^3 (this value includes the effects of iron catalyst) and $\rho_{PVA} = 1300$ kg/m^3. A detailed description of the experimental methods and spinning parameters is given in the Methods section.

While the parameter space associated with this procedure is large, once the apparatus is built, the only spinning parameters that can easily be varied are the concentration of the nanotube suspension, C_{NT}, and the PVA and SWNT flow rates, $\dot{V}_{PVA}$ and $\dot{V}_{SWNT}$. Initially, we prepared fibers with various diameters and nanotube volume fractions by spinning with various combinations of C_{NT}, $\dot{V}_{PVA}$, and $\dot{V}_{SWNT}$. However, it became apparent that the final fiber diameter scaled linearly with $\dot{V}_{SWNT}/\dot{V}_{PVA}$ (Figure S2A in Supporting Information). In addition, we found that V_f scaled approximately linearly with D, as shown in Figure S2B ($V_f \propto D^a$, $a = 0.93 \pm 0.25$), a correlation that is probably due to the details of the spinning process. This allowed some control of the final fiber properties. We prepared a range of different fibers with varying D (~1 to ~15 μm) and V_f (2−31%). Three of these fibers were drawn to a range of draw ratios (up to 63%). In all cases, the dried fibers were very uniform along their length, as shown in Figure 1A. In addition, the cross sections were close to circular (Figure 1B inset). On tensile fracture, large quantities of nanotube bundles were observed protruding from the broken ends (Figure 1B).

Mechanical Properties. Stress−strain curves were measured for all fibers using Zwick Z100 and Textechno Favimat tensile testers. Shown in Figure 1C are stress−strain curves for a $V_f = 26.5\%$ fiber, drawn to 0, 15, and 61% ($D = 10.2$, 8.6, and 6.3 μm, respectively). It is clear from this figure that the ultimate tensile strength, σ_B, and modulus, Y, increase on drawing. However, in this case, the strain at break, ε_B, tends to fall off with drawing. The stress-strain curve for a very low D fiber ($D = 1.4$ m) is shown for comparison in Figure

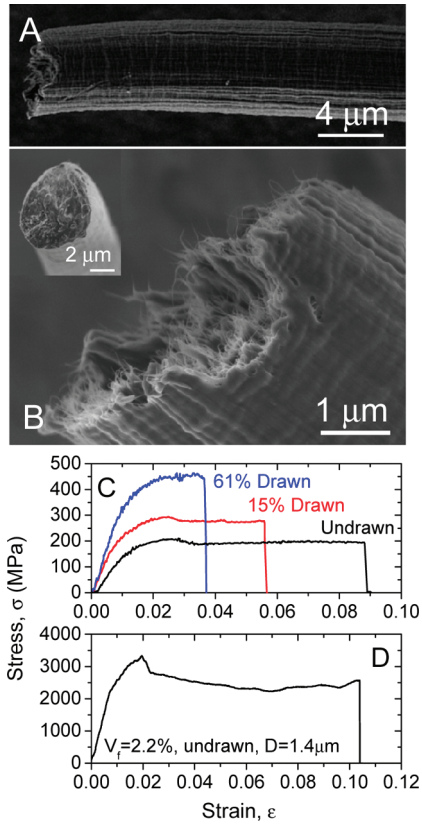

Figure 1. (A,B) SEM images of coagulation spun polymer-nanotube composite fibers (V_f = 26.5%, drawn DR = 15%). (C) Stress-strain curves for fiber with V_f = 26.5%, drawn to 0, 15, and 61% (D = 10.2, 8.6, and 6.3 μm, respectively). (D) Stress-strain curve for the strongest fiber studied (V_f = 2.2%, undrawn, D = 1.4 μm).

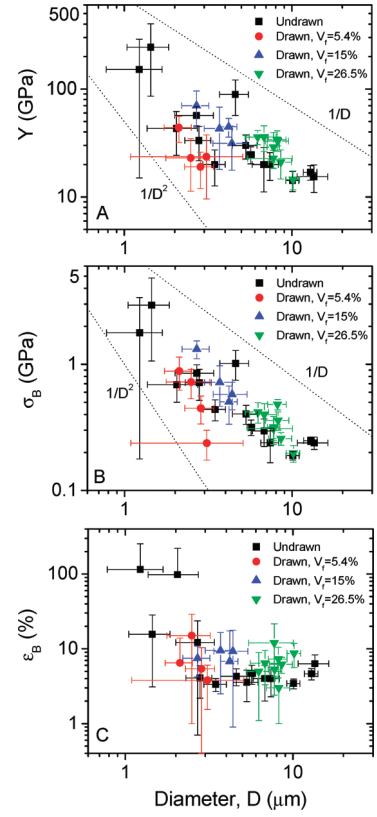

Figure 2. Mechanical properties of composite fibers as a function of fiber diameter. (A) Young's modulus, (B) ultimate tensile strength, and (C) strain at break. The data set marked undrawn consists of a range of different fibers with different diameters and a range of nanotube volume fractions between 2 and 31%. The data sets marked drawn consist of fibers of a given volume fraction, drawn to different DR values (and so different diameters). In (A) and (B), the dotted lines represent D^{-1} and D^{-2} behavior and have been included for reference.

1D. For all fibers measured, σ_B, Y, and ε_B were recorded (as well as D and V_f). We have previously shown that, for PVA−SWNT fibers, both σ_B and Y scale in direct proportion with V_f in agreement with eqs 1 and 2.[27] However, the dependence of σ_B, Y, and ε_B on fiber diameter has not been widely reported for polymer−nanotube fibers.[39] Shown in Figure 2A−C are Y, σ_B, and ε_B, respectively, plotted as a function of fiber diameter, D. In each case, the data are separated into undrawn fibers and drawn fibers (three different V_f). From these data, it is clear that both Y and σ_B scale strongly with D. The mean modulus scales from ~15 ± 4 GPa for large D fibers (~13 μm) to 244 ± 160 GPa for very low D fibers (D = 1.4 ± 0.7 μm, V_f = 2.2%). To our knowledge, the stiffest coagulation spun polymer-nanotube composite fiber had Y ~ 80 GPa,[12] while low diameter electrospun fibers[40] have been reported with moduli up to 85 GPa. Similarly, the mean strength scales from 190 ± 15 MPa for large D fibers (~10 μm) to 2.9 ± 1.9 GPa for very low D fibers (D = 1.4 ± 0.7 μm, V_f = 2.2%). These high mean strengths are consistent with similar fibers reported by Dalton *et al.*[12] (1.8 GPa), Miaudet *et al.*[18] (1.6 GPa), and Minus *et al.*[19] (2.6 GPa). We note that the strongest individual (rather than average over ~10 individuals) fiber we observed had σ_B = 3.5 ± 1.7 GPa (D = 1.4 ± 0.7 μm, V_f = 2.2%, Figure 1D). This exceeds the strongest previously reported coagulation spun PVA−SWNT fiber, which displayed σ_B = 2.6 GPa.[19] The trend is less clear for the strain at break. However, ε_B appears to decrease with decreasing D before increasing again at diameters below ~5 μm. (Note that the errors in Y and σ_B quoted above for the low D fibers are largely due to the spread in diameter measurements. Given that failure is more likely in low D regions of the fiber, the negative parts of the error bars are probably overestimated.)

The data shown in Figure 2 are quite scattered simply because all of the reported fibers had different nanotube volume fractions. As both Y and σ_B scale linearly with V_f, this will mask the true diameter dependence. In addition, as V_f scales with D (see above), fibers with higher D tend to have higher V_f and are thus stiffer and stronger. This results in the undrawn data appearing to have a different slope in Figure 2A,B compared to the drawn data. We can remove the effects of varying volume fraction by noting that we can approximate the modulus and strength as scaling in direct proportion to the vol-

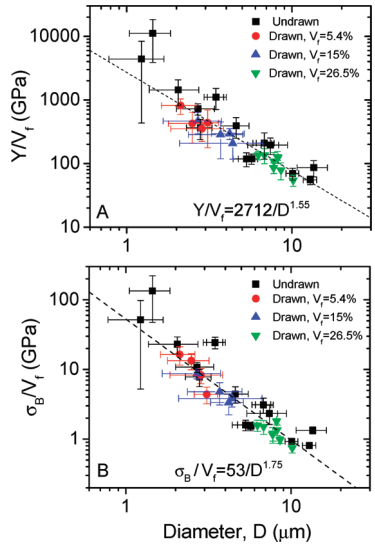

Figure 3. Same data as in Figure 2A,B. However, in this case, the modulus and strength have been divided by the fiber volume fraction. We expect that the resultant parameter will be very close to the rate of increase of mechanical properties with volume fraction, dY/dV_f and $d\sigma_B/dV_f$ (better agreement expected for larger diameter fibers).

ume fraction (eqs 1 and 2). This means we can correct for varying V_f by dividing both Y and σ_B by V_f. The added advantage of this procedure is that Y/V_f and σ_B/V_f can be thought of as measures of the degree of the reinforcement achieved (*i.e.*, approximately equivalent to dY/dV_f and $d\sigma_B/dV_f$).[7] However, we note that the approximation in eqs 1 and 2 is only correct if the composite is much stronger/stiffer than the polymer alone. While this is generally the case, it may break down for high-performance fibers with highly aligned polymer chains. In that case, the mechanical contribution of the matrix is much more important than that of the nanotubes.[41] While we have shown the approximation to hold for fibers with $D \sim 5-10$ μm,[27] some of the lower diameter fibers studied in this work may display some chain alignment and therefore higher than expected stiffness and strength. This could mean that $Y/V_f > dY/dV_f$ and $\sigma_B/V_f > d\sigma_B/dV_f$ for the very low D fibers.

As described in the introduction, the upper limits achievable are $Y/V_f \approx Y_{NT} = 1$ TPa and $\sigma_B/V_f \approx \sigma_{NT} \approx 100$ GPa. We note that in some publications Y/V_f and σ_B/V_f are referred to as Y_{Eff} and σ_{Eff}, respectively. Shown in Figure 3 are Y/V_f and σ_B/V_f plotted as a function of D. It is clear that the scatter is much reduced in each case. The mean modulus data vary from $Y/V_f = 55 \pm 8$ GPa ($D = 13$ μm) to $Y/V_f = 11 \pm 7$ TPa ($D = 1.4 \pm 0.7$ μm). Similarly, the mean strength data vary from $\sigma_B/V_f = 800 \pm 55$ MPa ($D = 13$ μm) to $\sigma_B/V_f = 134 \pm 65$ GPa ($D = 1.4 \pm 0.7$ μm). We note that the highest observed values of Y/V_f (11 TPa) are significantly higher than the expected maximum. This has been observed before[19,32,40] and may indicate the presence of nanotube-templated crystallinity. In addition, the maximum value of σ_B/V_f (134 GPa) is extremely high compared to the majority of values reported in the literature. However, it is also possible that such low diameter fibers tend to have well-aligned polymer chains, resulting in $Y/V_f > dY/dV_f$ and $\sigma_B/V_f > d\sigma_B/dV_f$ as described above. Further studies will be required to test this possibility.

The data shown in Figure 3 appear to be well-described by power laws of the form $Y/V_f \propto D^{-u}$ and $\sigma_B/V_f \propto D^{-v}$. By fitting the data, we obtain $u = 1.55 \pm 0.2$ and $v = 1.75 \pm 0.2$. Remarkably, the data for both undrawn and drawn fibers lie on the same curve. This is interesting as it suggests that the fiber diameter rather than the mechanism (drawing or spinning) is the controlling factor which determines the diameter. Given that $V_f \propto D^{0.93\pm0.25}$, this means for a given V_f, $Y \propto D^{-0.62\pm0.45}$ and $\sigma_B \propto D^{-0.82\pm0.45}$.

ANALYSIS AND DISCUSSION

It is important to try to understand the nature of the diameter dependence. It will be easiest to discuss the fiber strength first. In fact, the tensile strength of most fibers tends to scale with fiber diameter.[30,42−46] The simplest model proposed to explain this behavior is Smook's[47] modification of Griffith's model for stress enhancement due to surface flaws.[48] However, this model does not match the observed diameter dependence (Figure S3 in Supporting Information).

Fiber Strength: Defects. Perhaps more common are statistical models based on defect-induced fracture. The Weibull model[49] assumes that defects are homogeneously distributed throughout the material and failure at the most serious flaw leads to total failure of the material.[42,44,50] Within this framework, the probability of failure of a sample under a stress, σ, is given by

$$P(\sigma) = 1 - \exp\left[-n\left(\frac{\sigma}{\sigma_0}\right)^b\right] \qquad (3)$$

where n is the number of flaws present (Weibull originally considered fracture of a chain of n links with fracture occurring at the weakest link[49]), σ_0 is the scale factor, and b is the Weibull modulus. Generally, $P(\sigma)$ is approximated by ranking a set of breaking stresses (strengths) measured for a given fiber type in ascending order (in this work, for each fiber type, we typically tested 10 fiber sections, each of gauge length $L_0 = 10$ mm). Then the probability of failure is taken as the i-th stress in a group of N measurements as $P(\sigma) = i/(N + 1)$. Equation 3 can be rewritten as

$$\ln[-\ln(1 - P(\sigma))] = \ln(n/\sigma_0^b) + b \ln \sigma \qquad (4)$$

Thus, plotting $\ln[-\ln(1 - P(\sigma))]$ *versus* $\ln \sigma$ allows one to find b. This is important because it can be shown that the mean strength, σ_B, is given by $\sigma_B = \sigma_0 n^{-1/b}\Gamma(1 + 1/b)$, where Γ is the gamma function.[42] For any real sample, the flaws may be on the surface or distributed

in the bulk. This means that n is proportional to either the sample surface area or volume, respectively. Thus the mean fiber strength is given by

$$\sigma_B = \sigma_0\left(\frac{N}{A}\pi D L_0\right)^{-1/b}\Gamma(1 + 1/b) \quad (5)$$

or

$$\sigma_B = \sigma_0\left(\frac{N}{V}\frac{\pi}{4}D^2 L_0\right)^{-1/b}\Gamma(1 + 1/b)$$

depending on the location of the dominant flaw (*i.e.*, surface or bulk), where N/A and N/V are the surface and bulk flaw densities and L_0 is the gauge length. This is important to us as it shows that $\sigma_B \propto D^{-\alpha/b}$, where α is 1 or 2, depending on the flaw type. We can find b for our fibers by measuring the breaking stress a number of times for each fiber type and analyzing the data using eq 4. We have done this analysis for all fibers studied. An example of this is shown in Figure 4A for a $V_f = 5.4\%$ fiber drawn to different draw ratios. In all cases, a very good fit was obtained giving values of b close to 3.5 in all cases. No dependence of b on V_f was observed. Overall, we found $b = 3.5 \pm 0.5$, averaging over all samples (see Figure S4 in Supporting Information). We note that this value is very close to the value of $b = 3.4$ reported by Liu *et al.* for electrospun polymer−nanotube fibers.[16] These values are relatively small compared to the values of $b \sim 27$ reported for polyethylene fibers,[42] illustrating that the failure stress distribution is relatively broad in these PVA-SWNT composite fibers.

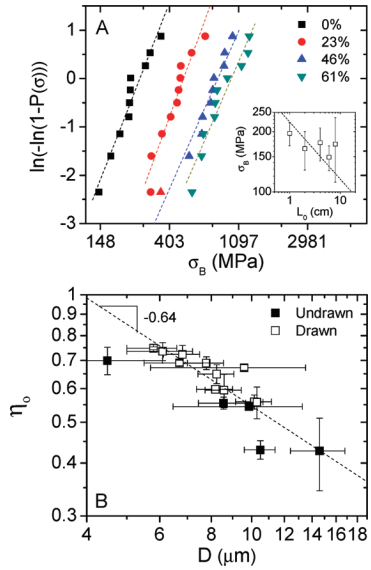

Figure 4. (A) Weibull analysis of the distribution of fiber breaking stresses for a given fiber type. Here $P(\sigma)$ is approximately the probability that the fiber will fracture at a given stress, σ. In this figure, the Weibull analysis has been carried out for fibers of volume fraction $V_f = 5.4\%$, drawn to different degrees. The inset shows the strength plotted as a function of gauge length, L_0, for undrawn fibers. In this case, $D = 11.5$ μm and $V_f = 11\%$. The dashed line has a slope of $-1/b = -1/3.5$. (B) Krenchel's orientation parameter plotted as a function of fiber diameter for both drawn and undrawn fibers.

We can test the Weibull analysis by noting that according to eq 5, $\sigma_B \propto L_0^{-1/b}$, where L_0 is the gauge length of the fiber under study. We performed mechanical tests on fibers with identical diameter and volume fraction ($D = 11.5$ μm, $V_f = 11\%$) at range of gauge lengths from 1 to 10 cm. The fiber strength is plotted *versus* gauge length in the inset of Figure 4A, showing a slight decrease in strength with increasing gauge length. The dashed line illustrates the type of dependence expected if the Weibull analysis is appropriate and taking $b = 3.5$ ($\sigma_B \propto L_0^{-1/3.5}$). While the agreement is not perfect, the data are certainly consistent with the Weibull analysis within the error bounds.

Having measured b, we can compare the dependence of fiber strength on diameter predicted by the Weibull analysis with the data in Figure 3B. To do this, we need the D dependence of σ_B/V_f. Remembering that V_f scales with D ($V_f \propto D^a$, $a = 0.93 \pm 0.25$), this means $\sigma_B/V_f \propto D^{-\alpha/b-a}$. From our values of b and a, we calculate $\alpha/b + a$ to be 1.2 ± 0.5 for $\alpha = 1$ and 1.5 ± 0.5 for $\alpha = 2$. Both of these values are compatible with our measurements of σ_B as a function of D ($\sigma_B/V_f \propto D^{-(1.75\pm0.2)}$), with the volumetric flaw scenario ($\alpha = 2$) a much closer match. However, this is unlikely to be the final answer. This is because the model described above works best for homogeneous fibers, made from a single component such as polyethylene[42,51] or SiC.[52]

Fiber Strength: Nanotube Orientation. However, the fibers under study in this work are polymer−nanotube composite fibers. In such structures, the strength is strongly correlated with the nanotube orientation distribution. This is represented in eq 2 by η_o, Krenchel's orientation parameter.[53] This parameter can vary from $\eta_o = 0$ for the nanotubes aligned in-plane perpendicular to the applied stress to $\eta_o = 0.2$ for randomly aligned nanotubes to $\eta_o = 1$ for nanotubes perfectly aligned in the direction of the applied stress. For fibers with diameters on the order tens of micrometers or lower, the nanotubes tend to become partially aligned during fiber spinning.[36,37] Such alignment is expected to increase as D decreases. Thus, we expect η_o and so σ_B to vary with D due to orientation effects. This is in addition to any flaw-related diameter dependence.

Wagner has proposed that eq 3 can be modified slightly to account for orientation effects by introducing a diameter dependence to the Weibull scale parameter, $\sigma_0 \propto D^{-\gamma}$.[44] This means a new component of diameter dependence is added to the fiber strength, allowing us to rewrite eq 5, including the dependence of V_f on D:

$$\sigma_B/V_f \propto D^{-\alpha/b-a}D^{-\gamma} \quad (6)$$

where $\alpha/b + a$ is 1.2 ± 0.5 for $\alpha = 1$ and 1.5 ± 0.5 for $\alpha = 2$. Here, the $D^{-\alpha/b}$ part represents the effect of flaws while the $D^{-\gamma}$ part represents the effects of nanotube orientation (the D^{-a} part represents the diameter de-

pendence of the volume fraction). By comparing eqs 2 and 6, we can associate $D^{-\gamma}$ with the diameter dependence of η_o:

$$\eta_o(D) \propto D^{-\gamma} \quad (7)$$

For the effects of defects and nanotube orientation to fully explain the observed diameter dependence, it will be necessary to show that eq 6 accurately describes the data presented in Figure 3B. For this to occur, the experimentally measured exponents must balance:

$$v = \frac{\alpha}{b} + a + \gamma \quad (8)$$

where v is the experimentally measured exponent: $\sigma_B/V_f \propto D^{-v}$ ($v = 1.75 \pm 0.2$). This requires $\gamma = 0.25 \pm 0.7$ for bulk defects ($\alpha = 2$) or $\gamma = 0.55 \pm 0.7$ for surface defects ($\alpha = 1$). We emphasize that v, b, and a were measured independently by measuring the tensile strength as a function of diameter, from the Weibull analysis and from the scaling of volume fraction with fiber diameter, respectively. To test our defect/orientation hypothesis, it will be necessary to measure the diameter dependence of η_0 in our fibers.

It is possible to obtain information on the nanotube alignment using Raman spectroscopy.[54] This makes use of the fact that the observed Raman intensity depends on the angle between the nanotube axis and the electric field vector of the excitation beam.[55] By measuring the Raman signals with the incident beam polarized parallel and perpendicular to the fiber, it is possible to calculate[56] the Herman's orientation parameter, S, where

$$S = [3\langle\cos^2\theta\rangle - 1]/2 \quad (9)$$

and θ is the angle between a given nanotube and the fiber axis (see Supporting Information for details, S2 and Figure S5). This orientation parameter varies from $S = -0.5$ for rods aligned in-plane to $S = 0$ for random orientation to $S = 1$ for perfect axial alignment. We measured S for a number of undrawn fibers of varying diameters between 4.5 and 14.6 μm, giving values from 0.72 to 0.38, respectively. In addition, we measured S for one fiber type, drawn to different draw ratios. The diameter was measured for all draw ratios. Here S scaled from 0.39 to 0.77 as drawing reduced the diameter from 10.5 to 5.8 μm. In order to obtain η_o for these fibers, we calculated both S and η_o for Gaussian distributions of fibers with a range of angular widths (see Supporting Information and Figure S6). By fitting these data, we found an empirical relationship between S and η_o:

$$\eta_o = 0.19 + 0.52S + 0.26S^2 \quad (10)$$

This expression gives η_o to an accuracy of 0.01 or better. Thus, for this subset of fibers, we have data for η_o as a function of D. These data are plotted in Figure 4B. Here we see η_o increase from 0.43 to 0.75 as D is decreased from 15 to 5.8 μm. Notably, both the as-spun and drawn data follow the same curve, showing that the orientation distribution is controlled by D. The data follow a clear power law as predicted by eq 7, with exponent $\gamma = 0.64 \pm 0.1$. This agrees extremely well with the requirement outlined above that $\gamma = 0.55 \pm 0.7$ for surface defects ($\alpha = 1$). (We note that all exponents are summarized in Table 1.)

1

exponent	parameter controlled	value
a	volume fraction, $V_f \propto D^a$	$a = 0.93 \pm 0.25$
u	fiber modulus (measured), $Y/V_f \propto D^{-u}$	$u = 1.55 \pm 0.2$
v	fiber strength (measured), $\sigma_B/V_f \propto D^{-v}$	$v = 1.75 \pm 0.2$
α/b	strength (defects), $\sigma_B \propto D^{-\alpha/b}$	$\alpha/b = 0.29 \pm 0.04$ ($\alpha = 1$, surface defects)
γ	strength (orientation), $\sigma_B \propto D^{-\gamma}$	$\gamma = 0.64 \pm 0.1$

It is worth noting that such behavior can also be seen in the data of other researchers. Both Badaire *et al.*[36] and Pichot *et al.*[37] prepared PVA−SWNT coagulation spun fibers which they characterized by X-ray scattering. They reported the fwhm of the nanotube distribution as a function of DR. We have calculated η_o for their fibers, which we have plotted *versus* D (Figure S7). These data show the sort of power law behavior predicted by eq 7, although notably with exponents significantly different than ours ($\gamma = 1.19$ and 1.17, respectively). This shows that the details of the nanotube distribution are set by the spinning parameters and apparatus.

Young's Modulus. The Young's modulus of fibers does not tend to be as susceptible to defects as the strength is. However, the modulus will depend on nanotube orientation as described by eq 1. As described above, it is now possible to separate the effects of defects from those due to the nanotube orientation. The orientation dependence is described by the exponent γ, thus we expect the modulus to scale with D as $Y/V_f \propto D^{-a-\gamma}$, where a accounts for the dependence of V_f on D. We have already measured $a = 0.93 \pm 0.25$ and $\gamma = 0.64 \pm 0.1$, giving $a + \gamma = 1.57 \pm 0.35$. However, we have already measured the diameter dependence of the modulus: $Y/V_f \propto D^{-u}$, where we obtain $u = 1.55 \pm 0.2$. The agreement between observed and predicted modulus exponents is almost perfect.

We can use the Young's modulus data shown in Figure 3A, coupled with the relationship between η_o and D, to check that the measured moduli (and hence the measured stresses in general) are in the correct range. By plotting Y/V_f *versus* η_o, we can use equation 1 to estimate $Y_{NT} \sim 235$ GPa (see Figure S8). This is more or less as expected (a value somewhat less than 1000 GPa) and agrees reasonably well with our previous estimate of 480 GPa.[27]

Relative Contribution of Orientation and Defects. It is worth briefly considering the relative contributions of defect and nanotube orientation to fiber strength. For a given V_f, the actual fiber strength depends on D as $\sigma_B \propto D^{-\alpha/b-\gamma}$. As we have seen, the data indicate that $\alpha = 1$, suggesting that surface defects initiate failure. This allows us to write the diameter dependence numerically as $\sigma_B \propto D^{-0.29}D^{-0.64}$, where the first term describes the defect contribution while the second term describes the orientation contribution. This clearly shows that nanotube orientation is more important than the presence of surface flaws in the fibers studied here. We note that the balance may be different for other types of fiber or indeed coagulation spun fibers produced using different spinning parameters.

It is important to realise that this diameter dependence should not apply over the entire diameter range. While the defect contribution should hold over a wide D range, the orientation dependence should only apply over the limited range of diameters where $0.2 < \eta_o < 1$. Outside this range, the nanotubes will either be randomly orientated or completely aligned. By extrapolating the $\eta_o(D) \propto D^{-\gamma}$ curve, we find that this η_o range is equivalent to 4 μm $< D <$ 50 μm. Thus, we expect coagulation spun fibers with $D >$ 50 μm to have completely randomly aligned nanotubes and commensurately poor mechanical properties. For $D <$ 4 μm, Y should be diameter independent (no orientation or defect effects) with $Y/V_f \propto D^{-a}$. In addition, the orientation component of σ_B should have saturated for $D <$ 4 μm, leaving a weaker defect controlled diameter dependence (*i.e.*, $\sigma_B/V_f \propto D^{-\alpha/b-a}$). This means we should expect to see two well-defined regions in the data in Figure 3A,B. This is not observed, possibly due to polymer chain alignment effects discussed above. On the other hand, the effect may be present but obscured by the error bars and residual scatter.

CONCLUSIONS

In conclusion, we have characterized the mechanical properties of polymer−nanotube fibers as a function of fiber diameter. We observed a strong dependence of fiber modulus and strength on diameter. This D dependence is a combination of the effects of nanotube orientation and surface defects. We have determined the balance of these effects and show that orientation effects are dominant for fiber diameters between 4 and 50 μm. For low diameter fibers, where the nanotubes are well-aligned, we have prepared fibers with mean moduli approaching 250 GPa and mean strength of 2.9 GPa.

While the defect contribution to the diameter dependence is relatively small ($D^{-0.29}$), this could probably be reduced dramatically by improving the spinning process. Better processing should reduce the surface defect density and increase b dramatically. The orientation contribution to the diameter dependence is larger ($D^{-0.64}$). However, it should be possible to change γ by changing the processing conditions (Pichot *et al.* and Badaire *et al.* reported data consisted of $\gamma = 1.17$ and $\gamma = 1.19$, respectively). A reduction of γ, possibly by optimization of needle and pipe diameters and flow rates, would reduce the orientation contribution to the diameter dependence. Such improvements could result in extremely high stiffness and strength for higher diameter fibers.

METHODS

Purified SWNTs (HiPCO, Unidym), polyvinylalcohol (J. T Baker, M_w = 77 000−79 000 g mol^{-1}), and the surfactant sodium cholate (Aldrich) were all used as supplied. A surfactant solution was prepared by dissolving sodium cholate in deionized water at 1 wt % (10 mg mL^{-1}) and stirring overnight. SWNTs were dispersed in this solution at 0.35 wt % (3.5 mg mL^{-1}) using a sonic tip processor (GEX600, 48 W, 24 kHz, flat head probe) operated in pulsed mode (1 s on/1 s off) for 7.5 h. The resulting nanotube dispersion was mildly centrifuged at 5500 rpm for 90 min (Hettich EBA12) to give a stock solution. The mean length and diameter of the bundles in the stock were measured by atomic force microscopy to be 315 and 1.8 nm, respectively (see Figure S1 in Supporting Information). The absorption spectra (Cary 6000i UV−vis−IR spectrometer) measured before and after centrifugation were compared to calculate SWNT concentration in the stock. The stock dispersion was diluted with surfactant solution (1 wt %) to give a range of nanotube concentrations from 0.07 and 0.35 wt %. A 5 wt % (50 mg mL^{-1}) solution of polyvinylalcohol in deionized water was prepared as the coagulant by stirring and then refluxed at approximately 110 °C until it became transparent (3−5 h).

To prepare the fibers, the surfactant-dispersed, single-walled nanotubes (SWNTs) were injected at well-defined flow rates into the center of a cylindrical pipe (inner diameter 5 mm) in which the polyvinylalcohol solution flowed. Contact with the PVA solution caused collapse of the nanotube dispersion into a continuous nanotube−PVA fiber, which then traveled down the pipe to be collected on a mandrel in a water bath. The fiber length was limited only by the supply of the NT dispersion. The fibers collected from the mandrel contained very large quantities of water: we refer to them as wet-state precursor fibers. They were cut into sections and removed from the bath for drying, initially at ambient conditions and then under vacuum for 48 h. The diameter of the fibers after drying was in the range of 1−15 μm. Some experiments were performed on as-spun fibers that were undrawn. In other cases, the wet-state precursor fibers were drawn by attaching them to two rollers on a custom-built rack. The rollers could be controllably rotated, resulting in the drawing of the fibers to well-defined draw ratios, DR (DR = $(L - L_0)/L_0$). After drawing, the fibers were dried as described above.

Thermogravimetric analysis (Perkin-Elmer Pyris 1) was used to calculate the nanotube mass fraction of a subset of fibers. Scanning electron microscopy (SEM) was performed using a Hitachi S-4300 field emission scanning electron microscope. Mechanical testing was performed with a Zwick Z100 tensile tester using a 100 N load cell with a strain rate of 1 mm min^{-1}. The gauge length was generally kept constant at 10 mm (except for gauge length experiments). The sensitivity of this instrument in this force range was verified by testing Kevlar fibers of similar di-

ameter and known strengths. In order to check the accuracy of this instrument, some low diameter fibers were also tested using a Textechno Favimat tensile tester with a 2 N load cell. For each sample, mechanical tests were made on 10 fibers and the mean and standard deviation of the relevant mechanical parameters calculated. A Renishaw 2000 system equipped with a 633 nm He−Ne laser was used to record Raman spectra of the fibers. The laser spot size was 2 μm in diameter, and the power was 0.5 mW when the laser was focused on the fiber.

Acknowledgment. The authors thank Science Foundation Ireland for financial support through the Principle Investigator scheme, Grant Number 07/IN.1/I1772.

Supporting Information Available: S1, table of fiber properties; S2, measurement of S; S3, calculation of η_o and S, supporting figures. This material is available free of charge *via* the Internet at http://pubs.acs.org.

REFERENCES AND NOTES

1. Belytschko, T.; Xiao, S. P.; Schatz, G. C.; Ruoff, R. S. Atomistic Simulations of Nanotube Fracture. *Phys. Rev. B* **2002**, *65*, 235430.
2. Li, C. Y.; Chou, T. W. A Structural Mechanics Approach for the Analysis of Carbon Nanotubes. *Int. J. Solids Struct.* **2003**, *40*, 2487–2499.
3. Lu, J. P. Elastic Properties of Single and Multilayered Nanotubes. *J. Phys. Chem. Solids* **1997**, *58*, 1649–1652.
4. Lu, J. P. Elastic Properties of Carbon Nanotubes and Nanoropes. *Phys. Rev. Lett.* **1997**, *79*, 1297–1300.
5. Yakobson, B. I.; Campbell, M. P.; Brabec, C. J.; Bernholc, J. High Strain Rate Fracture and C-Chain Unraveling in Carbon Nanotubes. *Comput. Mater. Sci.* **1997**, *8*, 341–348.
6. Yu, M. F.; Files, B. S.; Arepalli, S.; Ruoff, R. S. Tensile Loading of Ropes of Single Wall Carbon Nanotubes and Their Mechanical Properties. *Phys. Rev. Lett.* **2000**, *84*, 5552–5555.
7. Coleman, J. N.; Khan, U.; Blau, W. J.; Gun'ko, Y. K. Small but Strong: A Review of the Mechanical Properties of Carbon Nanotube−Polymer Composites. *Carbon* **2006**, *44*, 1624–1652.
8. Kannan, P.; Young, R. J.; Eichhorn, S. J. Debundling, Isolation, and Identification of Carbon Nanotubes in Electrospun Nanofibers. *Small* **2008**, *4*, 930–933.
9. Andrews, R.; Jacques, D.; Rao, A. M.; Rantell, T.; Derbyshire, F.; Chen, Y.; Chen, J.; Haddon, R. C. Nanotube Composite Carbon Fibers. *Appl. Phys. Lett.* **1999**, *75*, 1329–1331.
10. Chae, H. G.; Sreekumar, T. V.; Uchida, T.; Kumar, S. A Comparison of Reinforcement Efficiency of Various Types of Carbon Nanotubes in Poly Acrylonitrile Fiber. *Polymer* **2005**, *46*, 10925–10935.
11. Chen, X. Y.; Beyerlein, I. J.; Brinson, L. C. Curved-Fiber Pull-out Model for Nanocomposites. Part 1: Bonded Stage Formulation. *Mech. Mater.* **2009**, *41*, 279–292.
12. Dalton, A. B.; Collins, S.; Munoz, E.; Razal, J. M.; Ebron, V. H.; Ferraris, J. P.; Coleman, J. N.; Kim, B. G.; Baughman, R. H. Super-Tough Carbon-Nanotube Fibres—These Extraordinary Composite Fibres Can Be Woven into Electronic Textiles. *Nature* **2003**, *423*, 703.
13. Gao, J. B.; Itkis, M. E.; Yu, A. P.; Bekyarova, E.; Zhao, B.; Haddon, R. C. Continuous Spinning of a Single-Walled Carbon Nanotube−Nylon Composite Fiber. *J. Am. Chem. Soc.* **2005**, *127*, 3847–3854.
14. Haggenmueller, R.; Fischer, J. E.; Winey, K. I. Single Wall Carbon Nanotube/Polyethylene Nanocomposites: Nucleating and Templating Polyethylene Crystallites. *Macromolecules* **2006**, *39*, 2964–2971.
15. Kumar, S.; Dang, T. D.; Arnold, F. E.; Bhattacharyya, A. R.; Min, B. G.; Zhang, X. F.; Vaia, R. A.; Park, C.; Adams, W. W.; *et al.* Hauge Synthesis, Structure, and Properties of PBO/SWNT Composites. *Macromolecules* **2002**, *35*, 9039–9043.
16. Liu, L. Q.; Tasis, D.; Prato, M.; Wagner, H. D. Tensile Mechanics of Electrospun Multiwalled Nanotube/Poly(methyl,ethacrylate) Nanofibers. *Adv. Mater.* **2007**, *19*, 1228.
17. Ma, W. K. A.; Chinesta, F.; Ammar, A.; Mackley, M. R. Rheological Modeling of Carbon Nanotube Aggregate Suspensions. *J. Rheol.* **2008**, *52*, 1311–1330.
18. Miaudet, P.; Badaire, S.; Maugey, M.; Derre, A.; Pichot, V.; Launois, P.; Poulin, P.; Zakri, C. Hot-Drawing of Single and Multiwall Carbon Nanotube Fibers for High Toughness and Alignment. *Nano Lett.* **2005**, *5*, 2212–2215.
19. Minus, M. L.; Chae, H. G.; Kumar, S. Interfacial Crystallization in Gel-Spun Poly(vinyl alcohol)/Single-Wall Carbon Nanotube Composite Fibers. *Macromol. Chem. Phys.* **2009**, *210*, 1799–1808.
20. Mu, M.; Winey, K. I. Improved Load Transfer in Nanotube/Polymer Composites with Increased Polymer Molecular Weight. *J. Phys. Chem. C* **2007**, *111*, 17923–17927.
21. Sandler, J. K. W.; Pegel, S.; Cadek, M.; Gojny, F.; van Es, M.; Lohmar, J.; Blau, W. J.; Schulte, K.; Windle, A. H.; Shaffer, M. S. P. A Comparative Study of Melt Spun Polyamide-12 Fibres Reinforced with Carbon Nanotubes and Nanofibres. *Polymer* **2004**, *45*, 2001–2015.
22. Vigolo, B.; Penicaud, A.; Coulon, C.; Sauder, C.; Pailler, R.; Journet, C.; Bernier, P.; Poulin, P. Macroscopic Fibers and Ribbons of Oriented Carbon Nanotubes. *Science* **2000**, *290*, 1331–1334.
23. Vigolo, B.; Poulin, P.; Lucas, M.; Launois, P.; Bernier, P. Improved Structure and Properties of Single-Wall Carbon Nanotube Spun Fibers. *Appl. Phys. Lett.* **2002**, *81*, 1210–1212.
24. Hull, D.; Clyne, T. W. *An Introduction to Composite Materials*; Cambridge University Press: New York, 1996.
25. Rosenthal, J. A Model for Determining Fiber Reinforcement Efficiencies and Fiber Orientation in Polymer Composites. *Polym. Composite* **1992**, *13*, 462–466.
26. Wang, Z.; Ciselli, P.; Peijs, T. The Extraordinary Reinforcing Efficiency of Single-Walled Carbon Nanotubes in Oriented Poly(vinyl alcohol) Tapes. *Nanotechnology* **2007**, *18*, 455709.
27. Blighe, F. M.; Young, K.; Vilatela, J. J.; Windle, A. H.; Kinloch, I. A.; Deng, L.; Young, R. J.; Coleman, J. N. The Effect of Nanotube Content and Drawing on the Mechanical Properties of Coagulation-Spun Polymer−Nanotube Composite Fibres: Separating Intrinsic Reinforcement from Orientational Effects. *Adv. Funct. Mater.* DOI: 10.1002/adfm.201000940.
28. Bergin, S. D.; Nicolosi, V.; Streich, P. V.; Giordani, S.; Sun, Z. Y.; Windle, A. H.; Ryan, P.; Niraj, N. P. P.; Wang, Z. T. T.; Carpenter, L.; *et al.* Towards Solutions of Single-Walled Carbon Nanotubes in Common Solvents. *Adv. Mater.* **2008**, *20*, 1876.
29. Kearns, J. C.; Shambaugh, R. L. *J. Appl. Polym. Sci.* **2002**, 86.
30. Chae, H. G.; Choi, Y. H.; Minus, M. L.; Kumar, S. Carbon Nanotube Reinforced Small Diameter Polyacrylonitrile Based Carbon Fiber. *Compos. Sci. Technol.* **2009**, *69*, 406–413.
31. Coleman, J. N.; Cadek, M.; Ryan, K. P.; Fonseca, A.; Nagy, J. B.; Blau, W. J.; Ferreira, M. S. Reinforcement of Polymers with Carbon Nanotubes. The Role of an Ordered Polymer Interfacial Region. Experiment and Modeling. *Polymer* **2006**, *47*, 8556–8561.
32. Coleman, J. N.; Cadek, M.; Blake, R.; Nicolosi, V.; Ryan, K. P.; Belton, C.; Fonseca, A.; Nagy, J. B.; Gun'ko, Y. K.; Blau, W. J. High-Performance Nanotube-Reinforced Plastics: Understanding the Mechanism of Strength Increase. *Adv. Funct. Mater.* **2004**, *14*, 791–798.
33. Munoz, E.; Dalton, A. B.; Collins, S.; Kozlov, M.; Razal, J.; Coleman, J. N.; Kim, B. G.; Ebron, V. H.; Selvidge, M.; Ferraris, J. P.; *et al.* Multifunctional Carbon Nanotube Composite Fibers. *Adv. Eng. Mater.* **2004**, *6*, 801–804.
34. Razal, J. M.; Coleman, J. N.; Munoz, E.; Lund, B.; Gogotsi, Y.; Ye, H.; Collins, S.; Dalton, A. B.; Baughman, R. H. Arbitrarily Shaped Fiber Assemblies from Spun Carbon Nanotube Gel Fibers. *Adv. Funct. Mater.* **2007**, *17*, 2918–2924.

35. Poulin, P.; Vigolo, B.; Launois, P. Films and Fibers of Oriented Single Wall Nanotubes. *Carbon* **2002**, *40*, 1741–1749.
36. Badaire, S.; Pichot, V.; Zakri, C.; Poulin, P.; Launois, P.; Vavro, J.; Guthy, C.; Chen, M.; Fischer, J. E. Correlation of Properties with Preferred Orientation in Coagulated and Stretch-Aligned Single-Wall Carbon Nanotubes. *J. Appl. Phys.* **2004**, *96*, 7509–7513.
37. Pichot, V.; Badaire, S.; Albouy, P. A.; Zakri, C.; Poulin, P.; Launois, P. Structural and Mechanical Properties of Single-Wall Carbon Nanotube Fibers. *Phys. Rev. B* **2006**, 74.
38. Miaudet, P.; Bartholome, C.; Derre, A.; Maugey, M.; Sigaud, G.; Zakri, C.; Poulin, P. Thermo-Electrical Properties of PVA−Nanotube Composite Fibers. *Polymer* **2007**, *48*, 4068–4074.
39. Sui, X. M.; Wagner, H. D. Tough Nanocomposites: The Role of Carbon Nanotube Type. *Nano Lett.* **2009**, *9*, 1423–1426.
40. Almecija, D.; Blond, D.; Sader, J. E.; Coleman, J. N.; Boland, J. J. Mechanical Properties of Individual Electrospun Polymer−Nanotube Composite Nanofibers. *Carbon* **2009**, *47*, 2253–2258.
41. Deng, L.; Young, R. J.; van der Zwaag, S.; Picken, S. Characterization of the Adhesion of Single-Walled Carbon Nanotubes in Poly(*p*-phenylene terephthalamide) Composite Fibres. *Polymer* **2010**, *51*, 2033–2039.
42. Amornsakchai, T.; Cansfield, D. L. M.; Jawad, S. A.; Pollard, G.; Ward, I. M. The Relation between Filament Diameter and Fracture Strength for Ultra-High-Modulus Polyethylene Fibers. *J. Mater. Sci.* **1993**, *28*, 1689–1698.
43. Ji, Y.; Li, B. Q.; Ge, S. R.; Sokolov, J. C.; Rafailovich, M. H. Structure and Nanomechanical Characterization of Electrospun PS/Clay Nanocomposite Fibers. *Langmuir* **2006**, *22*, 1321–1328.
44. Wagner, H. D. Dependence of Fracture-Stress Upon Diameter in Strong Polymeric Fibers. *J. Macromol. Sci. B* **1989**, *B28*, 339–347.
45. Wagner, H. D. Stochastic Concepts in the Study of Size Effects in the Mechanical Strength of Highly Oriented Polymeric Materials. *J. Polym. Sci. Polym. Phys.* **1989**, *27*, 115–149.
46. Arinstein, A.; Burman, M.; Gendelman, O.; Zussman, E. Effect of Supramolecular Structure on Polymer Nanofibre Elasticity. *Nat. Nanotechnol.* **2007**, *2*, 59–62.
47. Smook, J.; Hamersma, W.; Pennings, A. J. The Fracture Process of Ultrahigh Strength Polyethylene Fibers. *J. Mater. Sci.* **1984**, *19*, 1359–1373.
48. Griffith, A. A. The Phenomena of Rupture and Flow in Solids. *Philos. Trans. R. Soc. London, Ser. A* **1921**, *A221*, 163.
49. Weibull, W. A Statistical Distribution Function of Wide Applicability. *J. Appl. Mech.* **1951**, *18*, 293–297.
50. Doremus, R. H. Fracture Statistics—A Comparison of the Normal, Weibull, and Type-I Extreme Value Distributions. *J. Appl. Phys.* **1983**, *54*, 193–198.
51. Karbhari, V. M.; Wilkins, D. J. Significance of Longitudinal and Transversal Size Effects on the Statistics of Fiber Strength. *Philos. Mag. A* **1991**, *64*, 1331–1344.
52. Lissart, N.; Lamon, J. Statistical Analysis of Failure of Sic Fibres in the Presence of Bimodal Flaw Populations. *J. Mater. Sci.* **1997**, *32*, 6107–6117.
53. Krenchel, H. *Fibre Reinforcement: Theoretical and Practical Investigations of the Elasticity and Strength of Fibre-Reinforced Materials*; Akademisk forlag, **1964**.
54. Kannan, P.; Eichhorn, S. J.; Young, R. J. Deformation of Isolated Single-Wall Carbon Nanotubes in Electrospun Polymer Nanofibres. *Nanotechnology* **2007**, 18.
55. Duesberg, G. S.; Loa, I.; Burghard, M.; Syassen, K.; Roth, S. Polarized Raman Spectroscopy on Isolated Single-Wall Carbon Nanotubes. *Phys. Rev. Lett.* **2000**, *85*, 5436–5439.
56. Liu, T.; Kumar, S. Quantitative Characterization of Swnt Orientation by Polarized Raman Spectroscopy. *Chem. Phys. Lett.* **2003**, *378*, 257–262.